BIOCHEMISTRY
including biophysical chemistry & molecular biology

Article

pubs.acs.org/biochemistry

Boundary of the Nucleotide-Binding Domain of *Streptococcus* ComA Based on Functional and Structural Analysis

Seiji Ishii,*[,†] Takato Yano,*[,§] Akihiro Okamoto,[∥] Takeshi Murakawa,[†] and Hideyuki Hayashi[†,‡]

[†]Department of Biochemistry and [‡]Department of Chemistry, Faculty of Medicine and [§]Biochemistry, Faculty of Nursing, Osaka Medical College, Osaka 569-8686, Japan

[∥]Department of Biological Science and Technology, High-Technology for Human Welfare, Tokai University, Shizuoka 410-0395, Japan

Supporting Information

ABSTRACT: The ATP-binding cassette (ABC) transporter ComA is a key molecule essential for the first step of the quorum-sensing system of *Streptococcus*. The nucleotide binding domains (NBD) of *Streptococcus mutans* ComA with different N termini, NBD1 (amino acid residues 495−760), NBD2 (517−760), and NBD3 (528−760), were expressed, purified, and characterized. The shortest NBD3 corresponds to the region commonly defined as NBD in the database searches of ABC transporters. A kinetic analysis showed that the extra N-terminal region conferred a significantly higher ATP hydrolytic activity on the NBD at a neutral pH. Gel-filtration, X-ray crystallography, and mutational analyses suggest that at least four to five residues beyond the N-terminal boundary of NBD3 indeed participate in stabilizing the protein scaffold of the domain structure, thereby facilitating the ATP-dependent dimerization of NBD which is a prerequisite to the catalysis. These findings, together with the presence of a highly conserved glycine residue in this region, support the redefinition of the N-terminal boundary of the NBD of these types of ABC exporters.

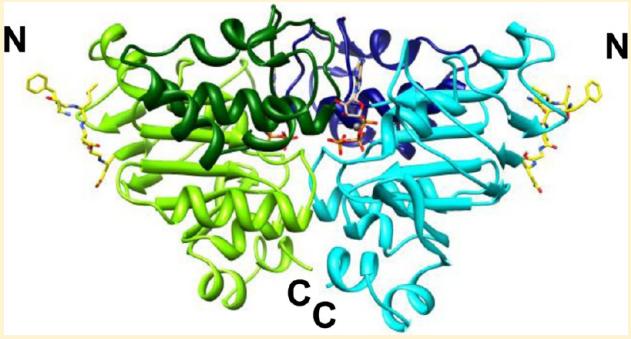

ATP-binding cassette (ABC) transporters form one of the largest protein superfamilies in many organisms and participate in a diversity of physiological functions, including virulence secretion,[1] multidrug resistance of tumor cells[2,3] and pathogenic bacteria,[4] antigen presentation,[5] and regulation of ion channels.[6] The typical core architecture of an ABC transporter is two transmembrane domains (TMD) and two cytosolic nucleotide-binding domains (NBD). The TMDs form the transport pathway with several membrane-spanning α-helices, which are divergent in sequence and number, reflecting the wide range of endogenous and exogenous ligands for the ABC transporters. On the other hand, the NBDs provide the driving force for substrate transport by their ATP hydrolytic activity and are conserved among the superfamily.

Despite the common organization of these domains, two TMDs and two NBDs are encoded in independent polypeptide chains and assembled together in most ABC *importers*, while in most ABC *exporters*, the dimers are formed from two polypeptide chains which are composed of the N-terminal TMD and the C-terminal NBD or from a single polypeptide chain with two TMD−NBD units fused in tandem.[7] Thus, for the ABC exporters, a linker region connects the TMD and NBD. Routinely, as in database searches, the boundaries in this linker region of the ABC exporters are defined by sequence comparisons with the N-termini of soluble single-domain−polypeptide NBDs of the ABC importers and other nucleotide triphosphatase superfamily members such as Rho GTPases and RecA.[8] There have been several studies where constructs with different N termini of NBDs of the ABC exporters were heterologously expressed in *Escherichia coli* to test the solubility of the protein products.[9−12] However, there have been no reports that discussed the exact domain boundary of NBD in terms of its detailed functional and structural properties.

ComA of *Streptococcus* is an essential ABC exporter for quorum-sensing signal transduction. Quorum-sensing is a bacterial cell−cell communication system mediated by an inherent small molecule to properly respond to environment changes and survive as a "community".[13] Bacterial cells sense the concentration increase of the secreted signal molecule in response to the change in the cell density by either the cell surface or intracellular receptors and then alter the target gene expression.[14,15] In *Streptococcus*, the quorum-sensing system is believed to regulate the competence for genetic transformation[16] and biofilm formation.[17−19] The competence-stimulating peptide, which functions as a quorum-sensing signal in this bacterium, is cleaved from the precursor peptide ComC and concomitantly exported to the extracellular space by ComA with a help of the accessory protein ComB. ComA is a member

Received: December 26, 2012
Revised: March 27, 2013
Published: March 27, 2013

of the ABC exporter maturation and secretion (AMS) protein family. This family features the N-terminal peptidase domain preceding the TMD, consisting of six membrane-spanning segments, and the C-terminal NBD located on the cytoplasmic face of the membrane.[20] We have recently characterized the peptidase domains from six species of *Streptococcus* and determined the three-dimensional structure of this domain from *S. mutans* at the near-atomic resolution of 1.9 Å.[21,22] It was also proposed that the peptidase domain of ComA recognizes ComC in a dual mode, in which a tight cleft in the vicinity of the active center binds the Gly−Gly cleavage motif and a shallow hydrophobic concave surface accommodates the conserved hydrophobic residues in the N-terminal region of ComC. On the other hand, little is known about the transport mechanism of the cleaved quorum-sensing peptide across the membrane, especially how the cleavage reaction and the transport are cooperated. To address this issue of interest, other parts of ComA, the TMD and the C-terminal NBD, should be investigated in isolation or in combinations with each other and the peptidase domain.

In this study, we found that the extra N-terminal region beyond the commonly annotated N-terminal boundary of NBD increased the ATPase activity and facilitated the dimerization of the NBD, which is essential for the catalysis. The crystal structure of the longest version of the NBD homodimer in complex with ATP-Mg^{2+} was then determined. The structure suggests that the N-terminus is located on the opposite side of the active site, but that a few residues of them are structurally integrated into the protein scaffold of the domain. This region contains a highly conserved glycine residue, and the replacement of this glycine with alanine impaired both the catalytic activity and the dimer formation. The present data would redefine the N-terminal boundaries of the NBDs of the ABC exporters.

EXPERIMENTAL PROCEDURES

Cloning and Plasmid Constructions of *S. mutans* NBDs. For the construction of the expression plasmids, the genes encoding the NBDs were directly amplified from the *S. mutans* (strain ATCC No. 700610) genomic DNA (GenBank AE014133) by PCR using the primers NBD1f and NBDr-his for bases 272110−272907, NBD2f and NBDr-his for bases 272176−272907, and NBD3f and NBDr-his for bases 272209−272907. The sequences of the primers used for the PCR are listed in Table S1. A His_6-tag sequence was attached to the C-terminal end of each NBD for the convenience of the purification. The PCR products were digested with *Nde*I and *Sal*I and ligated into pET21-b to generate pSMuN1, pSMuN2, and pSMuN3. The nucleotide sequences of the coding regions of all the expression plasmids were verified using an Applied Biosystems DNA sequencer, model 3130.

Site-Directed Mutagenesis. Mutagenesis was done using a QuikChange II site-directed mutagenesis kit (Stratagene) according to the manufacturer's instructions with pSMuN1 as the template. The primer pairs used for the mutagenesis are listed in Table S1. The nucleotide sequences of the entire coding regions were verified.

Protein Expression and Purification. For expression of the wild-type and mutant NBDs, an *E. coli* strain, BL21 (DE3) pLysS, was used as the host. The *E. coli* cells carrying each expression plasmid were grown overnight at 37 °C in LB medium containing 50 μg/mL ampicillin and 20 μg/mL chloramphenicol. The overnight culture of 3 mL was used to inoculate 600 mL of LB medium containing 50 μg/mL ampicillin and 20 μg/mL chloramphenicol, and the cells were grown with shaking at 37 °C for 2 h. For induction, isopropyl-β-D-thiogalactopyranoside was added to the culture to a final concentration of 0.2 mM, and the culture was allowed to grow at 37 °C for an additional 2 h. After the 2-h induction, the cultured medium was chilled in an ice−water bath, and the cells were harvested and resuspended in 12 mL of a buffer containing 20 mM Tris-HCl, 500 mM NaCl, and 5 mM imidazole, pH 7.9. The cell suspension was stored at −80 °C.

For protein purification, the cell suspension was thawed in a water bath, and then any insoluble material was removed by centrifuging at 15000*g* for 20 min at 4 °C. The supernatant was applied to a column packed with 1 mL of His·Bind Resin (Novagen). After the column was extensively washed with the above buffer containing 80 mM imidazole, the NBDs were eluted with a buffer containing 20 mM Tris-HCl, 500 mM NaCl, and 100 mM EDTA, pH 7.9. The eluate from the His·Bind column was dialyzed against a buffer containing 20 mM Tris-HCl, 150 mM NaCl, and 0.1 mM dithiothreitol (DTT), pH 7.0. G526A NBD1 used in the kinetic analysis was further purified using a Superose 12 10/300 GL column (GE Healthcare) connected to an ÄKTA fast protein liquid chromatography (FPLC) system (GE Healthcare) at the flow rate of 0.5 mL/min. The column was equilibrated and run with a buffer, 20 mM Tris-HCl, 150 mM NaCl, 0.1 mM DTT, pH 7.0. All the chromatography procedures were done at ambient temperature. The concentrations of the NBDs were spectrophotometrically determined based on the number of the aromatic amino acid residues.[23]

Circular Dichroism (CD) Measurements. The CD spectra of NBDs were recorded using a Jasco spectropolarimeter, model J-720WI (Jasco), equipped with a thermocontroller using a 0.1-cm light path sample cell. For the pH stability analysis, NBD in 20 mM Tris-HCl, 150 mM NaCl, 0.1 mM DTT, pH 7.0, was diluted with 39× volume of each of the following buffer solutions: 30 mM sodium acetate (for pHs 3.9 and 4.9), 30 mM sodium phosphate (for pHs 5.9, 6.9, and 7.9), or 30 mM sodium carbonate (for pHs 8.8 and 9.9) containing 150 mM NaCl. The final pH values were determined after CD measurements using a Horiba pH meter, model F-52 (Horiba). The CD spectra were measured at 25 °C.

Determination of Kinetic Parameters. The NBD's activity was assayed in a 100 μL reaction mixture containing 50 mM Tris-HCl, 150 mM NaCl, 10 mM $MgCl_2$, pH 8.5 or 7.0, and various concentrations of ATP. The ATP hydrolysis reaction was started by adding the NBD solution to a final protein concentration of 2.0 μM. The reaction was carried out at 25 °C, and 10 μL aliquots were transferred to wells of a 96-well plate containing 50 μL of BIOMOL GREEN reagent (Enzo Life Sciences) to quench the reaction and measure the inorganic phosphate at 620 nm by a microplate reader 680 XR (BIO-RAD). The data were analyzed using the Hill equation:

$$v = \frac{k_{cat}[E][S]^n}{{K_{0.5}}^n + [S]^n} \quad (1)$$

where v = velocity, k_{cat} = the catalytic rate, [E] = enzyme concentration, [S] = substrate concentration, $K_{0.5}$ = the concentration of substrate at 50% of the maximum velocity, and n = the Hill coefficient.

Gel-Filtration Analysis. A gel-filtration analysis was carried out using an ÄKTA FPLC system equipped with a Superose 12

dx.doi.org/10.1021/bi3017069 | *Biochemistry* 2013, 52, 2545−2555

10/300 GL column at the flow rate of 0.5 mL/min. The column was equilibrated and run with a buffer, 50 mM Tris-HCl, 150 mM NaCl, pH 8.5 or 7.0, containing various concentrations of ATP (and Mg^{2+}). The elution of NBD was monitored by the absorbance at 280 nm, and an elution volume was measured from the start of the sample application to the apex of each elution peak. The elution volume was calibrated using a gel-filtration calibration kit (GE Healthcare) containing ribonuclease A (13.7 kDa), carbonic anhydrase (29.0 kDa), ovalbumin (43.0 kDa), and conalbumin (75.0 kDa). The logarithm of the molecular mass was plotted versus K_{AV} that was calculated for each protein as follows:

$$K_{AV} = (V_e - V_0)/(V_t - V_0) \quad (2)$$

where V_e = elution volume for the protein, V_0 = column void volume, and V_t = total bed volume.

Protein Crystallization and Data Collection. NBD1 E690A was concentrated to about 7.5 mg/mL in 16.7 mM Tris-HCl, 125 mM NaCl, 12.5 mM ATP, and 0.083 mM DTT, pH 7.0, using a Vivaspin 6 centrifuge concentrator with a molecular mass cutoff of 10 kDa (Sartorius Stedim Biotech). Crystals were grown by sitting drop vapor diffusion. The protein solution containing 20 mM $MgCl_2$ was mixed with the precipitant solution containing 20% polyethylene glycol 8000, 0.1 M CAPS, pH 10.5, and 0.2 M NaCl at 4 °C in a 1:1 ratio. Crystals were observed on day 5. The crystals were briefly soaked in the precipitant solution with 22.5% glycerol and flash frozen in a liquid nitrogen stream (−173 °C). The crystallographic data were collected at BL44XU in SPring-8 (Hyogo, Japan) using a MX-225HE detector. The data sets were processed and scaled with the program package HKL 2000.[24]

Structure Determination and Analysis. The structure was solved by molecular replacement with MOLREP[25] using the homology model of NBD2 constructed from the crystal structure of TAP1 (PDB ID code 2IXE). Model building and refinement were performed with the programs REFMAC5,[26] COOT,[27] and PHENIX.[28] The refinement statistics are summarized in Supplemental Table S2, Supporting Information. The secondary structure elements were determined by the Stride program.[29] Figures were drawn using the program Chimera.[30] The atomic coordinates and structure factors have been deposited in the Protein Data Bank (www.rcsb.org/) under the accession code 3VX4.

RESULTS

Expression and Purification of ComA NBDs with Different N Termini. First, the boundaries of the TMD and NBD domains of *S. mutans* ComA were deduced by the CD-Search of the NCBI conserved domain database.[8] The database search predicted that the amino acid residues 212−482 and 528−760 of ComA are the TMD and the NBD, respectively. We then tried to heterologously express the NBDs with three different N termini: NBD1 (residues 495−760), NBD2 (517−760), and NBD3 (528−760). Each NBD could be expressed as a soluble protein in *E. coli* and purified to apparent homogeneity as judged on the SDS-polyacrylamide gels (Figure S1). The yields of the purified proteins from 300 mL of the bacterial culture were routinely ∼5.2 mg for NBD1; ∼ 1.1 mg for NBD2; and ∼2.3 mg for NBD3.

Before doing a detailed analysis on the isolated NBDs, the structural stability and folding properties of NBD1 were determined by circular dichroism (CD) measurements.[23] Figure S2 shows the CD values of NBD1 at 222 nm in the pH region of 4.9−9.9 measured immediately and at 24 h (kept at 25 °C) after the pH changes. The zero time data show that NBD1 is stable at pH > 5.9, although immediately denatured at pH 4.9. After 24 h, the CD values were identical to those at zero time at pH > 6.9, while the CD spectrum deteriorated at pH 5.9. Thus NBD1 is properly folded and stable enough for the analyses described below at neutral to alkaline pHs.

Kinetic Parameters of NBDs for ATP Hydrolysis. Generally, the ATP hydrolytic activities of the NBDs have been measured at either neutral[31,32] or alkaline pHs.[33,34] In this study, the kinetic parameters of NBD1, NBD2, and NBD3 for ATP hydrolysis were determined at pHs 8.5 and 7.0 (Table 1).

Table 1. Kinetic Parameters of NBDs for ATP at pHs 8.5 and 7.0[a]

NBDs	k_{cat} (min^{-1})	$K_{0.5}$ (mM)	$k_{cat}/K_{0.5}$ (M^{-1} s^{-1})	n
		pH 8.5		
NBD1	2.4 (0.075)	0.49 (0.028)	82	1.6 (0.097)
NBD2	1.6 (0.086)	0.35 (0.036)	76	1.7 (0.24)
NBD3	0.55 (0.026)	0.86 (0.061)	11	1.8 (0.17)
G526A NBD1	0.098 (0.0086)	1.2 (0.16)	1.4	1.9 (0.030)
		pH 7.0		
NBD1	1.2 (0.042)	0.49 (0.030)	41	1.7 (0.12)
NBD2	0.95 (0.024)	0.44 (0.020)	36	1.6 (0.087)
NBD3	0.059 (0.0063)	0.74 (0.12)	1.3	1.6 (0.24)
G526A NBD1	0.021 (0.0012)	0.53 (0.044)	0.66	2.2 (0.036)

[a]The experiments were carried out at 25 °C in 50 mM Tris-HCl, 150 mM NaCl, 10 mM $MgCl_2$, pH 8.5 or 7.0, as described in Experimental Procedures. The concentrations of ATP were 0.05−2 mM, except for 0.25−3 mM for NBD3 at pH 8.5 and 0.25−4 mM for G526A NBD1 at pH 8.5. The concentration of NBDs was 2.0 μM. Numbers in parentheses indicate the standard deviations.

The enzymatic activities were evaluated by measuring the initial rate of inorganic phosphate release at various ATP concentrations. The ATPase activity of the NBDs at these pHs did not follow the simple Michaelis−Menten kinetics in the [S]−v plot but displayed sigmoidal curves (Figure 1 for NBD1) with Hill coefficients (n) of 1.6−1.8. The catalytic rates (k_{cat}) of NBD1, NBD2, and NBD3 at pH 8.5 were 2-, 1.7-, and 9.3-fold higher than those at pH 7.0, respectively, whereas the $K_{0.5}$ values for

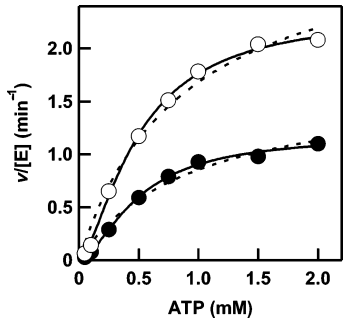

Figure 1. v/[E] versus substrate concentration plot of NBD1 for ATP. Different concentrations of ATP were hydrolyzed with 2.0 μM NBD1 in a buffer containing 50 mM Tris-HCl, 150 mM NaCl, at pH 8.5 (open circles) or 7.0 (closed circles) and 25 °C. Data points were fitted to a Michaelis−Menten equation (dashed line) or a Hill equation (solid line).

dx.doi.org/10.1021/bi3017069 | *Biochemistry* 2013, 52, 2545−2555

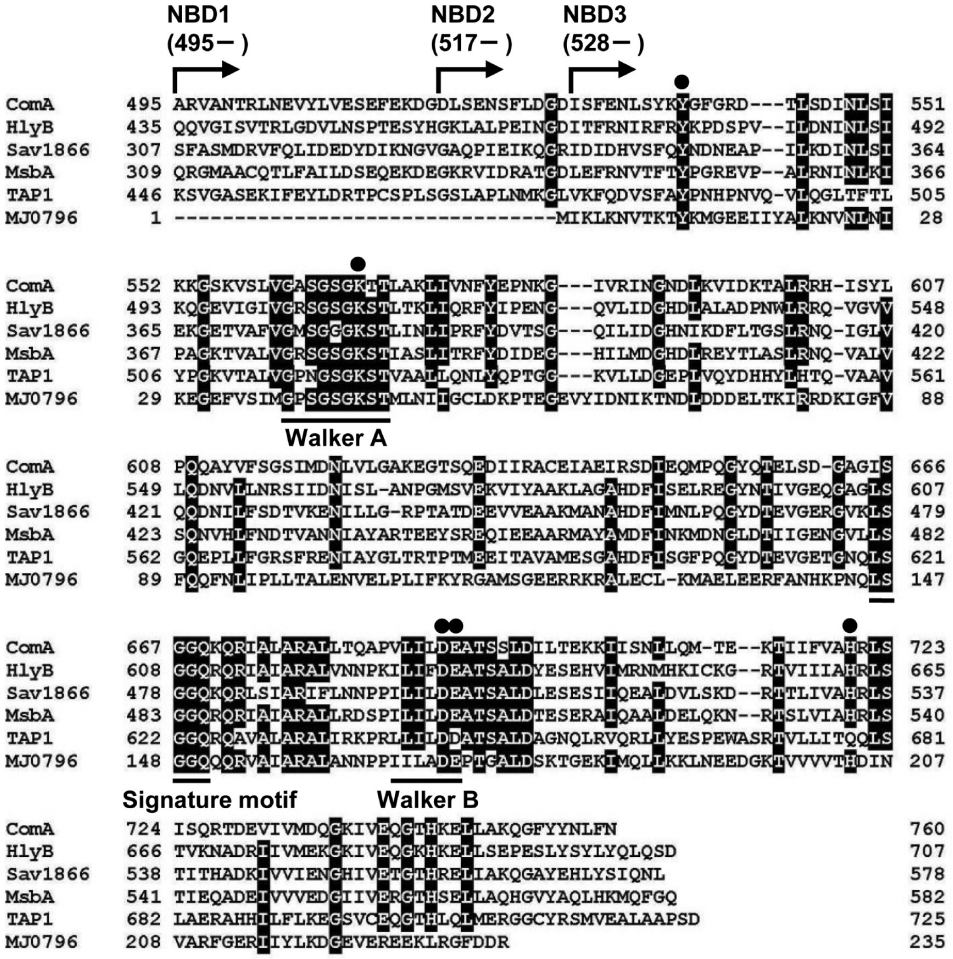

Figure 2. Amino acid sequence alignment of NBDs of ABC transporters. The amino acid residues that are identical in at least five of the compared NBD sequences are shaded black. *S. mutans* ComA; HlyB, the *E. coli* α-hemolysin transporter; Sav1866, the *Staphylococcus aureus* multidrug transporter; MsbA, the *Salmonella typhimurium* lipid flippase; TAP1, the rat antigen processing transporter; and MJ0796, the *Methanococcus jannaschii* LolD-homologue importer. Dots indicate five amino acid residues that are considered to be important for catalysis.

each NBD were identical at pHs 8.5 and 7.0. The catalytic efficiencies ($k_{cat}/K_{0.5}$) of NBD1 and NBD2 were almost comparable at both pHs. In contrast, the $k_{cat}/K_{0.5}$ values of NBD3 were 7.5- and 32-fold lower than those of NBD1 at pHs 8.5 and 7.0, respectively. These results clearly show that the N-terminal 11 amino-acid region (517–527) confers a high activity to the NBD, especially at neutral pH.

Conserved Active-Site Residues. As NBD1 exhibited the highest yield when expressed in *E. coli* and the highest ATPase activity, further analyses were done using this protein to characterize the NBD of ComA. Figure 2 shows the sequence alignment of the NBD of ComA with those of four ABC exporters and an ABC importer for which their three-dimensional structures are known. The NBD of ComA shows homologies in the region of 526–760 to those of the *E. coli* hemolysin exporter HlyB (45%), the *Staphylococcus aureus* multidrug exporter Sav1866 (41%), the *Salmonella typhimurium* lipid flippase MsbA (40%), the rat antigen processing transporter TAP1 (30%), and the LolD-homologue importer MJ0796 (29%) from *Methanococcus jannaschii*.

There are three major motifs commonly seen in the NBD domains of the ABC transporters, such as the Walker A motif (the region 561–569: GXXGXGKS/TT, where X is any amino acid), the Walker B motif (the region 685–690: ΦΦΦΦDE/D, where Φ is any hydrophobic amino acid), and the signature motif (the region 665–669: I/LSGGQ). In addition to these motifs, Tyr537 and His720 of ComA are supposed to be an adenine-ring stacking tyrosine and the H-loop histidine, respectively.[35] According to this alignment, the NBD of ComA is thought to be typical of the NBD domain of an ABC transporter. To experimentally confirm the importance of these motifs and also to identify a mutant NBD suitable for crystallization (see below), five conserved residues were selected, and the alanine mutations were introduced to measure the relative activities at a fixed ATP concentration of 2 mM at pH 8.5.

The activities of Y537A, E690A, and H720A NBD1s were significantly decreased (0.094–2.8%) in comparison to that of the wild-type NBD1, and K567A and D689A NBD1s exhibited a complete loss of activity (Table 2). Thus, the NBD of ComA should have structural and mechanistic features characteristic of the NBD domain of an ABC transporter.

ATP- and pH-Dependent Dimerization of the Wild-Type and Mutant NBDs. In order to examine the oligomeric state in the catalytic cycle of NBD, we carried out the gel-filtration assay of NBD1 in the absence or presence of ATP and/or Mg^{2+}. The NBD1 eluted with the ATP-free buffer at pHs 8.5 and 7.0 showed single, symmetrical peaks (Figure 3a,b,

dx.doi.org/10.1021/bi3017069 | *Biochemistry* 2013, 52, 2545–2555

Table 2. Relative Activities of the Wild-Type and Mutant NBD1s[a]

NBD1s	$v/[E]$ (min^{-1})	%/WT
WT	1.7	100
Y537A	0.048	2.8
K567A[b]	–	–
D689A[b]	–	–
E690A	0.0016	0.094
H720A	0.018	1.1

[a]Relative activities of NBD1s determined at a fixed substrate concentration of 2 mM ATP. The experiments were carried out at 25 °C in 50 mM Tris-HCl, 150 mM NaCl, 10 mM $MgCl_2$, pH 8.5, as described in Experimental Procedures. The concentration of the NBDs was 2.0 μM. Relative activities were determined by comparing the v/[E] of each mutant NBD to that of wild-type NBD. [b]The ATP hydrolysis could not be detected under the conditions described above.

red lines). The K_{AV} values approximately correspond to 31.0 and 29.2 kDa at pHs 8.5 and 7.0, respectively, based on the standard curves obtained with known proteins (Figure S3). Because the calculated molecular mass of NBD1 is 30.4 kDa, the ATP-free form of NBD1 is thought to exist as a monomer at these pHs.

When NBD1 was preincubated and eluted with the buffer containing various concentrations of ATP at pH 8.5, the peak was shifted toward lower elution volumes in an ATP-dependent manner up to the concentration of 5 mM (Figure 3a, magenta to blue lines). The peak elution volume of NBD1 in the presence of 10 mM ATP showed no more shifts, while the peak was further shifted upon the addition of 10 mM Mg^{2+} (Figure 3a, green line). Since the peak elution volume of the NBD1 dimer is estimated at 12.3 mL from the standard curve, these peak shifts toward lower elution volumes indicate the dimer formation of NBD1. The appearance of single peaks between the positions of the monomer and dimer forms, not double peaks with different heights corresponding to the two forms, indicates that the association and dissociation rates of the NBD subunits are significantly fast relative to the time scale for the chromatography (about 30 min). The monomer−dimer equilibrium of NBD1 at pH 7.0 was also shifted to the dimer by ATP or ATP-Mg^{2+}, but the extent of the shift was significantly smaller than that at pH 8.5 (Figure 3b). Reduction of the ATP concentration due to dilution or hydrolytic consumption by NBD1 would be negligible because the column was preequilibrated and eluted with the buffer containing the corresponding concentrations of ATP.

To check the effects of the active-site mutations on the dimerization and identify a promising candidate for crystallization, the same assay was done at pH 8.5 for the mutant NBD1s except D689A NBD1 whose expression level in *E. coli* was too low to be used in this experiment. The ATP-free forms of the K567A, E690A, and H720A NBD1s were eluted at 13.6 mL (Figure 3d−f, red lines). The peak of the ATP-free form of Y537A NBD1 was slightly shifted toward a lower elution volume, suggesting that the overall configuration of the monomer is somewhat altered upon this mutation (Figure 3c, red line). K567A failed to form the dimeric state by either ATP or ATP-Mg^{2+} (Figure 3d, blue and green lines). While the monomer−dimer equilibrium of Y537A NBD1 was not altered by ATP, it was shifted by ATP-Mg^{2+} (Figure 3c). For the E690A and H720A NBD1s, the dimer formation was slightly impaired in the presence of ATP alone, but the equilibrium was

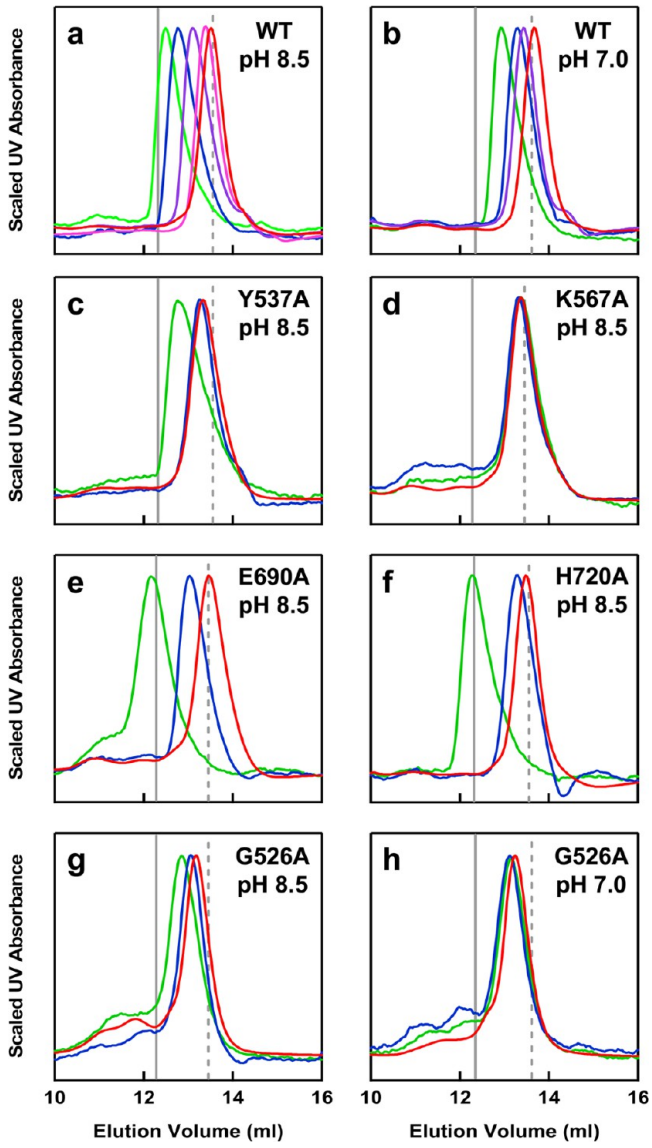

Figure 3. Analytical gel-filtration assay of NBD1s. Elution patterns for the wild-type (a and b) and mutant (c, Y537A; d, K567A; e, E690A; f, H720A; g and h, G526A) NBD1s in the absence (red) or presence of ATP (magenta, 0.5 mM; purple, 2.0 mM; blue, 5.0 mM ATP). Green lines indicate the elution patterns in the presence of 5.0 mM ATP and 10 mM $MgCl_2$. The protein solution contains 50 mM Tris-HCl, 150 mM NaCl, pH 8.5 (a, c, d, e, f, and g) or pH 7.0 (b and h), and corresponding concentrations of ATP (and Mg^{2+}). A 100 μL solution of 2.0 mg/mL of each NBD1 was applied onto a Superose 12 10/300 GL column and eluted with the same buffer at a flow rate of 0.5 mL/min at ambient temperature. The proteins were detected by monitoring the absorbance at 280 nm. Each elution pattern was subtracted with the buffer-baseline that did not contain the protein, and the ordinates of graphs were scaled for clarity of presentation. The baselines in this experiment were varied due to the UV absorption of the different ATP concentrations. Vertical solid and dashed lines are the calculated elution volumes corresponding to the dimer and monomer of NBD1, respectively (see text).

almost totally shifted toward the dimer by ATP-Mg^{2+} (Figure 3e,f). Additionally, although the E690A NBD1 was eluted as a symmetrical peak, other NBD1s including the wild type were eluted as tailing peaks in the presence of ATP and Mg^{2+}, indicating these proteins are dissociating into monomers during the elution. These observations implied that E690A NBD1

dx.doi.org/10.1021/bi3017069 | *Biochemistry* 2013, 52, 2545−2555

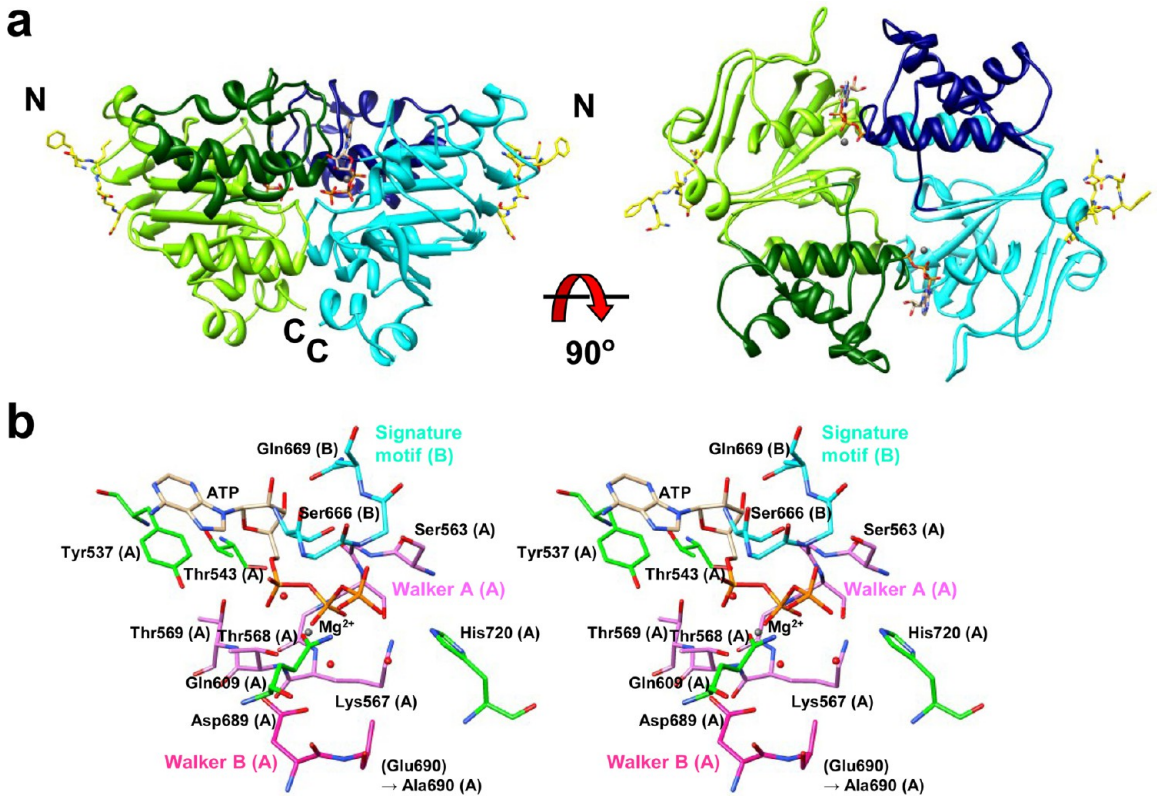

Figure 4. Structure of the E690A NBD1 homodimer complexed with ATP-Mg^{2+}. (a) Schematic representation of the overall structure of E690A NBD1. The secondary structure elements of the catalytic domain (the residues 528−608 and 683−760) and the helical domain (609−682) are colored light green and dark green, respectively, in the subunit A, and in cyan and dark blue, respectively, in the subunit B. The N-terminal residues 522−527 (subunit A) and 521−527 (subunit B) are colored yellow. The right structure is a view of the left one rotated by 90° along the *x*-axis. (b) Stereoview of the active site of E690A NBD1. The residues in the vicinity of the active site are indicated by sticks. The ATP, Mg^{2+}, and water are shown as white sticks, gray spheres, and red spheres, respectively. The oxygen, nitrogen, and phosphate atoms are colored red, blue, and orange, respectively. A and B in parentheses indicate the subunits to which each residue belongs. Glu690 is replaced with alanine in E690A NBD1.

formed the most stable dimer among the NBD1s in the presence of ATP and Mg^{2+}. Therefore, E690A NBD1 was selected for the cocrystallization with ATP-Mg^{2+}.

Overall Structure of the E690A NBD1 Homodimer. Crystals of E690A NBD1 were grown at 4 °C to suppress the ATP hydrolysis by the remaining activity. The crystal structure of E690A NBD1 in complex with ATP-Mg^{2+} was determined by molecular replacement at a 2.69 Å resolution with an R_{work} of 19.1% (R_{free} = 24.8%), and the root-mean square deviation (r.m.s.d.) from the ideal values in bond lengths and bond angles was 0.016 Å and 1.30°, respectively. No electron density was visible for a large part of the N-terminal residues (495−521 of the subunit A and 495−520 of the subunit B) and the C-terminal His tag. The final structure contains 479 amino acids with two ATP-Mg^{2+}'s and 148 water molecules. Further details of the crystallographic data and statistics are described in Table S2.

The E690A NBD1 monomer shows an L-shaped structure with two domains, which are generally referred to as the catalytic domain and the helical domain.[35] The larger catalytic domain (light shaded in Figure 4a) is composed of two β-sheets and six α-helices, which contains the Walker A and Walker B motifs. The smaller helical domain (dark shaded in Figure 4a) comprises a β-strand and five α-helices and contains the signature motif. Two monomers were assembled in head-to-tail configuration and two ATP-Mg^{2+} molecules are sandwiched at the interface between the subunits, and the N-terminal extension is located on the opposite site of the active center (yellow in Figure 4a).

The E690A NBD1 dimer has a Cα r.m.s.d. of 2.65 Å for 468 selected atoms and that of 1.97 Å for 400 selected atoms when compared to the HlyB H662A NBD dimer[36] and the MJ0796 E171Q NBD dimer,[37] respectively, using MIfit[38] (Figure 5a). The two subunits are not quite identical as is often observed in the NBDs of other ABC transporters.[39,40] The positional difference of the Cα atoms between the two subunits is plotted versus the residue number in Figure S4a. There are three remarkable differences except for the N- and C-terminal regions: positions 537−541 in the catalytic domain; and positions 611−637 and 646−664 in the helical domain. Consistently, in these regions, the B-factors of the A subunit are significantly larger than those of the B subunit (Figure S4b). These differences between the two subunits are probably caused by crystal packing. The buried surface area between the two E690A NBD1 monomers is 954 Å^2 (9% of total surface area of a monomer), calculated by AREAIMOL the program (CCP4 Program Suite). This value is 1440 Å^2 (13% of total surface area of a monomer) in the HlyB H662A NBD, which is similar in molecular size.[34]

Active-Site Structure of E690A NBD1. Each active site of the E690A NBD1 homodimer is composed of the conserved residues such as Tyr537, Thr543, Ser563−Thr569 of the Walker A motif, Gln609, Asp689 and the mutated Ala690 of the Walker B motif, and His720 of one subunit and Ser666−

dx.doi.org/10.1021/bi3017069 | *Biochemistry* 2013, 52, 2545−2555

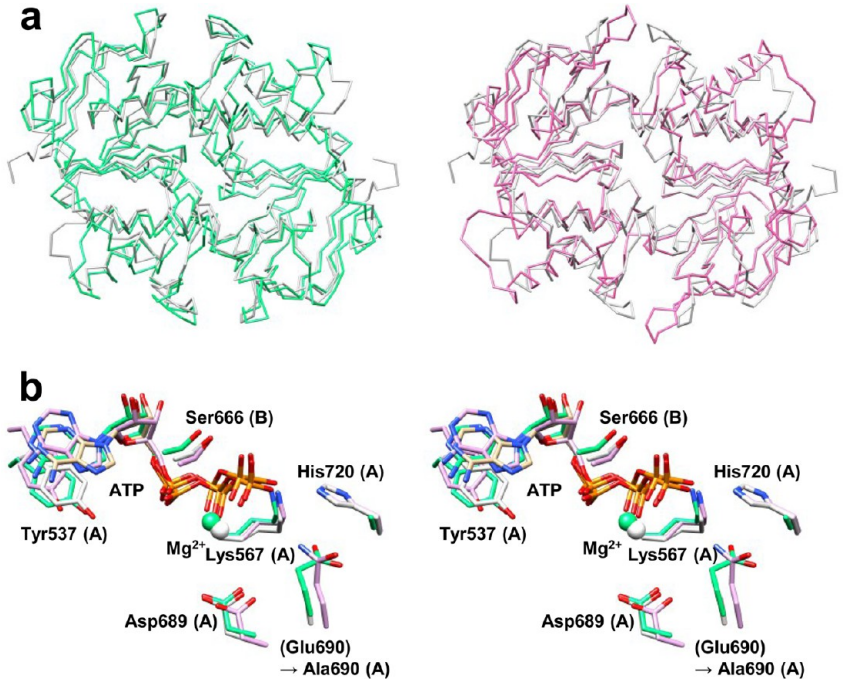

Figure 5. Structural comparisons of the E690A NBD1 dimer in complex with ATP-Mg^{2+} with the HlyB H662A NBD dimer in complex with ATP-Mg^{2+} (PDB ID code 1XEF) and the MJ0796 E171Q NBD dimer in complex with ATP (PDB ID code 1L2T). (a) The backbones of E690A NBD1 (gray) were superimposed with those of HlyB H662A NBD (light green, left) and MJ0796 E171Q NBD (magenta, right). (b) Stereoview of the active site superimpositions of E690A NBD1 with HlyB H662A NBD and MJ0796 E171Q NBD. The active-site residues of E690A NBD1, Y537, K567, D689, and A690 of the subunit A, S666 of the subunit B, ATP, and Mg^{2+} are shown by white color. The corresponding residues, ATP and Mg^{2+} of HlyB H662A NBD (light green) and MJ0796 E171Q NBD (magenta), are shown. The oxygen, nitrogen, and phosphate atoms are colored red, blue, and orange, respectively. A and B in parentheses indicate the subunits of E690A NBD1.

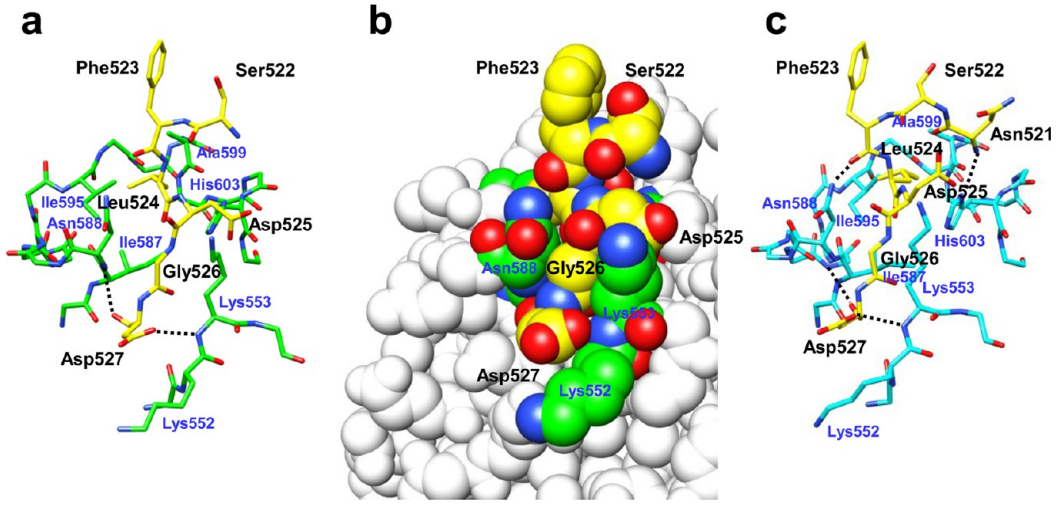

Figure 6. Interactions of the N-terminal extension of E690A NBD1 with the other part of the domain. Stick (a) and sphere (b) models of the residues 522−527 (yellow) and surrounding residues (green) in the subunit A. (c) Stick model of the residues 521−527 (yellow) and surrounding residues (cyan) in subunit B. Only the residues intimately interacting with the N-terminal extension region are depicted in (a) and (c). The oxygen and nitrogen atoms are colored red and blue, respectively. The dashed line indicates a hydrogen bond.

Gln669 of the signature motif of the opposed subunit (Figure 4b). The adenine ring of ATP forms a $\pi-\pi$ stacking interaction with the phenyl ring of Tyr537. The ribose moiety of ATP is accommodated with Thr543 and Gln669 with the hydrophobic interaction and hydrogen bond, respectively. The oxygen atoms of the α-, β-, and γ-phosphates of ATP are fixed by hydrogen bonds donated from main-chains and/or side-chains of Ser563−Thr569 of the Walker A motif, Gln609, His720, and Ser666 and Gly668 of the signature motif. A Mg^{2+} ion is octahedrally coordinated with the side-chains of Thr568 and Gln609, two oxygen atoms of the β- and γ-phosphates, and two water molecules. One of these coordinating water molecules makes a hydrogen bond with side-chain of Asp689. This architecture of the active site of E690A NBD1 is almost identical with those of HlyB H662A NBD and MJ0796 E171Q NBD (Figure 5b).

Environment around the N-Terminal Extension. Of particular interest in the present NBD structure is the detailed

dx.doi.org/10.1021/bi3017069 | *Biochemistry* 2013, 52, 2545−2555

environment around the N-terminal extension, especially the 11 amino-acid region corresponding to NBD2. Thus, the residue−residue interactions were determined using the PIC[41] and LIGPLOT[42] programs. In these regions, the residues 522−527 in subunit A and 521−527 in subunit B were visible (Figure 6). The backbone of residues 524−527 in subunit A is bound by the hydrophobic interactions with the imidazole ring of His603, the side-chain of Asn588, and the Cα atom and aliphatic side-chain of Lys553. Also, the side-chain of Leu524 is accommodated by a hydrophobic pocket constructed by the side-chains of Ile587, Ile595, and Ala599. The carbonyl oxygen of the main-chain and the carboxyl oxygen of the side-chain of Asp527 form hydrogen bonds with the main-chain amide nitrogens of Asn588 and Lys553, respectively. The ion-pairs exist between the side-chains of Asp525−Lys553, Asp525−His603, and Asp527−Lys552 (Figure 6a,b).

In subunit B, only the main-chains of Leu524 and Gly526 are bound by hydrophobic interactions with the imidazole ring of His603 and the Cα atom of Lys533, respectively (Figure 6c). There are, however, two more hydrogen bonds compared to those in the subunit A, which are formed between the main-chain amide of Asn521 and ND1 of His603, and the carbonyl oxygen of Phe523 and ND2 of Asn588. Other interactions, such as the hydrophobic interactions around the side-chain of Leu524 and the ion-pairs found in subunit A, also exist in this subunit (Figure 6c).

Overall, at least four to five residues of the N-terminal extension make intimate interactions with the surrounding residues and may constitute a part of the domain structure.

Effects of a Mutation Introduced in the N-Terminal Extension. The Gly526 of NBD1 was replaced with alanine. The $k_{cat}/K_{0.5}$ values decreased by 59- and 62-fold at pHs 8.5 and 7.0, respectively, due to this mutation (Table 1). Next, the gel-filtration assay was done to investigate the dimer formation of G526A NBD1. The peaks of G526A NBD1 in the absence of ATP were shifted toward lower elution volumes at pHs 8.5 and 7.0 compared to those of the wild-type NBD1 monomer (Figure 3g,h, red lines). Although the monomer−dimer equilibrium of G526A NBD1 was shifted toward the dimer formation in the presence of ATP or ATP-Mg^{2+} at pH 8.5 (Figure 3g, blue and green lines), these changes were significantly smaller than those of the wild-type NBD1. At pH 7.0, the dimer formation was not observed for G526A NBD1 in the presence of the same concentrations of ATP or ATP-Mg^{2+} (Figure 3h, blue and green lines).

DISCUSSION

Relationship between Dimerization and Catalysis. The Hill coefficients (n) of the three NBDs were all close to 2 at pHs 8.5 and 7.0 (Table 1). These results suggest a positive cooperativity between the two ATP binding sites in the NBD of ComA. In addition, the analytical gel-filtration assay demonstrated that the NBD monomers associate into the homodimer in an ATP dependent manner (Figure 3a,b). This finding was most evident in K567A NBD1 and E690A NBD1. The mutation of Lys567 of the Walker A motif resulted in a loss of activity and dimerization (Table 2 and Figure 3a,d) as previously reported for other NBDs, such as P-glycoprotein from mouse[43] and BmrA, a multidrug exporter from *Bacillus subtilis*.[44] Lys 567 interacts with the β- and γ-phosphates of ATP and would be particularly important for the ATP binding. Thus, K567A NBD would be unable to bind ATP, showing no ATP-dependent shift in the gel-filtration assay and loss of activity. The dimer of E690A NBD1 was apparently more stable than that of the wild-type NBD1 (Figure 3a,e). Similar results were obtained in the gel-filtration assay of other NBDs, such as MJ0796[45] and Glv, a glucose uptake importer from *Sulfolobus solfataricus*,[46] harboring mutations at the consensus glutamate residue at the end of the Walker B motif. The ATP hydrolytic activity of E690A NBD1 was significantly deteriorated (Table 2), and thus the E690A NBD1 seems to be effectively "locked" in the dimer state in the presence of ATP-Mg^{2+} (Figure 3e).

These findings indicate that the isolated NBD transiently associates into the productive dimer conformation upon ATP and Mg^{2+} binding, and then ATP is hydrolyzed, followed by dissociation into the monomers.

Relationship between pH Dependencies of Activity and Dimerization. The catalytic efficiencies of NBD1 and NBD2 at pH 8.5 are about 2-fold of those at pH 7.0, and the difference is more than 8-fold in NBD3 (Table 1 and Figure 1). NBD1 forms its dimer in an ATP-dependent manner more readily at pH 8.5 than at pH 7.0 (Figure 3a,b). The difference in the monomer−dimer equilibrium of NBD1 at pHs 8.5 and 7.0 well correlates with that in the activity at these pHs. Given the importance of the dimer formation during the catalysis, the readiness of dimerization seems to explain the reason why the activity is higher at pH 8.5 than at pH 7.0. To support this idea, it is desirable to confirm that the equilibrium of NBD3 is further shifted toward the monomer, especially at pH 7.0. However, NBD3 irreversibly stuck to the gel-filtration column, and no data could be obtained.

As for the amino acid residues responsible for the pH dependency of the dimer formation, we were unable to select specific ones, because there are too many potential residues at the subunit interface.

Domain Boundary of NBD. The precise N-terminal boundaries of the NBDs of the ABC exporters have rarely been discussed or experimentally explored. Domains corresponding to NBD3 (528−760) of ComA have routinely been annotated as NBD in database searches. Expression levels as soluble proteins when expressed in *E. coli* might be considered as an indicator of the domain boundaries but ideally should be accompanied by a more detailed analysis of the purified proteins. Here, three NBDs with different lengths were successfully overexpressed and purified in sufficient quantities, enabling us to do a comparative analysis.

Surprisingly, the ATP hydrolytic activity of NBD3 was significantly lower than those of NBD1 and NBD2 especially at pH 7.0, which is closer to the physiological conditions (Table 1). The relative activities among these three proteins did not correlate with the expression levels or yields of the purified proteins, supporting that the expression levels as soluble proteins are not reliable evidence for domain boundaries. The interesting question is how these extra N-terminal residues affect the ATP hydrolytic activity in spite of their locations at the opposite site of the active site. The three-dimensional structure of E690A NBD1 provided details surrounding this region. The residues 524−527 were fully integrated as a part of the globular domain structure (Figure 6). The main chain of this region, which precedes the first β-strand (528−531), bends at the position of Gly526 (Figure S5). Generally, a glycine residue has more conformational freedom than other amino acids and therefore can adopt many different conformations. Even a minimum change (Gly to Ala) at this position of NBD1 severely impaired the catalytic efficiency at pHs 8.5 and 7.0 (Table 1). The gel-filtration assay suggests that the overall

dx.doi.org/10.1021/bi3017069 | *Biochemistry* 2013, 52, 2545−2555

Figure 7. Structure-based sequence alignment of the residues 495−540 of ComA and the corresponding regions of other ABC exporters, of which full-length structures are known. Two completely conserved residues are marked with dots. The secondary structures are shown under the sequence. The α-helices and β-strands are represented as cylinders and arrows, respectively. Primary sequence of exporters, *S. mutans* ComA (this study), *Staphylococcus aureus* Sav1866 (PDB ID code 2ONJ), *Salmonella typhimurium* MsbA (PDB ID code 3B60), *Thermotoga maritima* TM287/288 heterodimer (PDB ID code 3QF4), and human P-glycoprotein (PDB ID code 3G5U), are aligned. As P-glycoprotein is the tandemly fused full-size transporter, the N-terminal NBD and the C-terminal NBD are designated as NBD1 and NBD2, respectively.

configuration of the G526A NBD1 monomer was slightly changed and that the dimer formation was impaired in this mutant NBD (Figure 3). Steric hindrance between the methyl group of alanine at this position and the side-chain of Asn588 would not be tolerated, and this mutation would destroy the regular secondary structure around residues 525−527. Thus, the alanine mutation at position 526 is thought to alter the static and/or dynamic conformations of the whole NBD domain. Similar effects might also be elicited by elimination of this region, that is the case in NBD3, thereby destabilizing the overall domain structure. This is supported by the low catalytic efficiency and the fact that NBD3 irreversibly sticks to the gel-filtration resin.

To date, three-dimensional structures of four full-length ABC exporters, such as Sav1866,[4] MsbA,[47] P-glycoprotein,[48] and TM287/288, a LmrCD-like multidrug exporter from *Thermotoga maritima*,[49] have been determined. A structure-based sequence alignment of ComA with these ABC exporters supports the importance of the region around Gly526 (Figure 7). The linker region composed of about 20 amino acids connects the last α-helix of TMD and the first β-strand of NBD. The glycine residue is completely conserved and is located near the C-terminal end of this linker and 11 amino-acid residues ahead of the adenine stacking tyrosine residue (Y537 in ComA) of the NBDs. Many NBDs from bacterial AMS proteins, human ABC exporters belonging to the ABCB or ABCC subfamily, and their relatives in bacteria and yeast listed in Figure S6 share this consensus sequence feature. Thus this glycine residue is thought to occupy a pivotal position in these ABC exporters. On the basis of the findings obtained in the present study, it is proposed that the annotation of NBD of the ABC exporters should include this glycine and probably up to three more N-terminal residues.

It is reasonable to infer that the three domains of ComA will cooperate during a round of peptide cleavage, ATP hydrolysis, and signal-peptide transport. This is the most interesting mechanistic question regarding the AMS family exporters. The findings obtained so far for the isolated peptidase domains and NBDs are far short of providing insights into this mechanism. Although it is obvious that studies on the full-length ComA are necessary and ideal, it is not technically feasible at present. Biochemical and biophysical studies of these domains and their substrates in various combinations at high protein concentrations would be the next step to achieve this purpose.

■ ASSOCIATED CONTENT

Supporting Information

Table S1 (oligonucleotides used in this article), Table S2 (X-ray data collection and refinement statistics), Figure S1 (purification of NBD1), Figure S2 (pH stability of NBD1), Figure S3 (gel-filtration analysis of NBD1), Figure S4 (structural differences between the subunits A and B of E690A NBD1), Figure S5 (structure of the region around Gly526), and Figure S6 (amino acid sequence alignment of NBDs of ABC exporters). This materials is available free of charge via the Internet at http://pubs.acs.org.

■ AUTHOR INFORMATION

Corresponding Author

*(S.I.) Address: Department of Biochemistry, Faculty of Medicine, Osaka Medical College, 2-7 Daigakumachi, Takatsuki, 569-8686, Japan. Tel.: 81-72-683-1221. Fax: 81-72-684-6516. E-mail: med002@art.osaka-med.ac.jp. (T.Y.) Address: Biochemistry, Faculty of Nursing, Osaka Medical College, 7-6 Hacchonishimachi, Takatsuki, 569-0095, Japan. Tel. and Fax.: 81-72-684-7281; E-mail: med013@art.osaka-med.ac.jp.

Funding

This work was supported by a grant from the Osaka Medical Research Foundation for Incurable Diseases (to T.M.).

Notes

The authors declare no competing financial interest.

■ ABBREVIATIONS USED

ABC, ATP-binding cassette; AMS, ABC exporter maturation and secretion; CD, circular dichroism; DTT, dithiothreitol; FPLC, fast protein liquid chromatography; NBD, nucleotide-binding domain; r.m.s.d, root-mean-square deviation; TMD, transmembrane domain

■ REFERENCES

(1) Lewis, V. G., Ween, M. P., and McDevitt, C. A. (2012) The role of ATP-binding cassette transporters in bacterial pathogenicity. *Protoplasma 249*, 919−942.

(2) Gottesman, M. M., and Ling, V. (2006) The molecular basis of multidrug resistance in cancer: the early years of P-glycoprotein research. *FEBS Lett. 580*, 998−1009.
(3) Pajic, M., Iyer, J. K., Kersbergen, A., van der, B. E., Nygren, A. O., Jonkers, J., Borst, P., and Rottenberg, S. (2009) Moderate increase in Mdr1a/1b expression causes in vivo resistance to doxorubicin in a mouse model for hereditary breast cancer. *Cancer Res. 69*, 6396−6404.
(4) Dawson, R. J., and Locher, K. P. (2006) Structure of a bacterial multidrug ABC transporter. *Nature 443*, 180−185.
(5) Procko, E., and Gaudet, R. (2009) Antigen processing and presentation: TAPping into ABC transporters. *Curr. Opin. Immunol. 21*, 84−91.
(6) Aittoniemi, J., Fotinou, C., Craig, T. J., de, W. H., Proks, P., and Ashcroft, F. M. (2009) Review. SUR1: a unique ATP-binding cassette protein that functions as an ion channel regulator. *Philos. Trans. R. Soc. Lond B Biol. Sci. 364*, 257−267.
(7) Davidson, A. L., Dassa, E., Orelle, C., and Chen, J. (2008) Structure, function, and evolution of bacterial ATP-binding cassette systems. *Microbiol. Mol. Biol. Rev. 72*, 317−64.
(8) Marchler-Bauer, A., and Bryant, S. H. (2004) CD-Search: protein domain annotations on the fly. *Nucleic Acids Res. 32*, W327−W331.
(9) de Araujo, E. D., Ikeda, L. K., Tzvetkova, S., and Kanelis, V. (2011) The first nucleotide binding domain of the sulfonylurea receptor 2A contains regulatory elements and is folded and functions as an independent module. *Biochemistry 50*, 6655−6666.
(10) Kerr, I. D., Berridge, G., Linton, K. J., Higgins, C. F., and Callaghan, R. (2003) Definition of the domain boundaries is critical to the expression of the nucleotide-binding domains of P-glycoprotein. *Eur. Biophys. J. 32*, 644−654.
(11) Baubichon-Cortay, H., Baggetto, L. G., Dayan, G., and Di Pietro, A. (1994) Overexpression and purification of the Carboxy-terminal nucleotide-binding domain from mouse P-glycoprotein. *J. Biol. Chem. 269*, 22983−22989.
(12) Dayan, G., Baubichon-Cortay, H., Jault, J. M., Cortay, J. C., Deléage, G., and Di Pietro, A. (1996) Recombinant N-terminal nucleotide-binding domain from mouse P-glycoprotein. *J. Biol. Chem. 271*, 11652−11658.
(13) Fuqua, W. C., Winans, S. C., and Greenberg, E. P. (1994) Quorum sensing in bacteria: the LuxR-LuxI family of cell density-responsive transcriptional regulators. *J. Bacteriol. 176*, 269−275.
(14) Fuqua, C., Parsek, M. R., and Greenberg, E. P. (2001) Regulation of gene expression by cell-to-cell communication: acyl-homoserine lactone quorum sensing. *Annu. Rev. Genet. 35*, 439−468.
(15) Miller, M. B., and Bassler, B. L. (2001) Quorum sensing in bacteria. *Annu. Rev. Microbiol. 55*, 165−199.
(16) Pestova, E. V., Håvarstein, L. S., and Morrison, D. A. (1996) Regulation of competence for genetic transformation in *Streptococcus pneumoniae* by an auto-induced peptide pheromone and a two-component regulatory system. *Mol. Microbiol. 21*, 853−862.
(17) Li, Y. H., Tang, N., Aspiras, M. B., Lau, P. C., Lee, J. H., Ellen, R. P., and Cvitkovitch, D. G. (2002) A quorum-sensing signaling system essential for genetic competence in *Streptococcus mutans* is involved in biofilm formation. *J. Bacteriol. 184*, 2699−2708.
(18) Petersen, F. C., Pecharki, D., and Scheie, A. A. (2004) Biofilm mode of growth of *Streptococcus intermedius* favored by a competence-stimulating signaling peptide. *J. Bacteriol. 186*, 6327−6331.
(19) Yoshida, A., and Kuramitsu, H. K. (2002) Multiple *Streptococcus mutans* Genes Are Involved in Biofilm Formation. *Appl. Environ. Microbiol. 68*, 6283−6291.
(20) Håvarstein, L. S., Diep, D. B., and Nes, I. F. (1995) A family of bacteriocin ABC transporters carry out proteolytic processing of their substrates concomitant with export. *Mol. Microbiol. 16*, 229−240.
(21) Ishii, S., Yano, T., Ebihara, A., Okamoto, A., Manzoku, M., and Hayashi, H. (2010) Crystal structure of the peptidase domain of *Streptococcus* ComA, a bifunctional ATP-binding cassette transporter involved in the quorum-sensing pathway. *J. Biol. Chem. 285*, 10777−10785.
(22) Kotake, Y., Ishii, S., Yano, T., Katsuoka, Y., and Hayashi, H. (2008) Substrate recognition mechanism of the peptidase domain of the quorum-sensing-signal-producing ABC transporter ComA from *Streptococcus*. *Biochemistry 47*, 2531−2538.
(23) Ishii, S., Yano, T., and Hayashi, H. (2006) Expression and characterization of the peptidase domain of *Streptococcus pneumoniae* ComA, a bifunctional ATP-binding cassette transporter involved in quorum sensing pathway. *J. Biol. Chem. 281*, 4726−4731.
(24) Otwinowski, Z., and Minor, W. (1997) Processing of X-ray diffraction data collected in oscillation mode. *Methods Enzymol. 276*, 307−326.
(25) Vagin, A., and Teplyakov, A. (2000) An approach to multi-copy search in molecular replacement. *Acta Crystallogr., Sect. D: Biol. Crystallogr. 56*, 1622−1624.
(26) Murshudov, G. N., Vagin, A. A., and Dodson, E. J. (1997) Refinement of macromolecular structures by the maximum-likelihood method. *Acta Crystallogr., Sect. D: Biol. Crystallogr. 53*, 240−255.
(27) Emsley, P., and Cowtan, K. (2004) Coot: model-building tools for molecular graphics. *Acta Crystallogr., Sect. D: Biol. Crystallogr. 60*, 2126−2132.
(28) Adams, P. D., Grosse-Kunstleve, R. W., Hung, L. W., Ioerger, T. R., McCoy, A. J., Moriarty, N. W., Read, R. J., Sacchettini, J. C., Sauter, N. K., and Terwilliger, T. C. (2002) PHENIX: building new software for automated crystallographic structure determination. *Acta. Crystallogr., Sect. D: Biol. Crystallogr. 58*, 1948−1954.
(29) Frishman, D., and Argos, P. (1995) Knowledge-based protein secondary structure assignment. *Proteins 23*, 566−579.
(30) Pettersen, E. F., Goddard, T. D., Huang, C. C., Couch, G. S., Greenblatt, D. M., Meng, E. C., and Ferrin, T. E. (2004) UCSF Chimera–a visualization system for exploratory research and analysis. *J. Comput. Chem. 25*, 1605−1612.
(31) Liu, C. E., Liu, P. Q., and Ames, G. F. (1997) Characterization of the adenosine triphosphatase activity of the periplasmic histidine permease, a traffic ATPase (ABC transporter). *J. Biol. Chem. 272*, 21883−21891.
(32) Syberg, F., Suveyzdis, Y., Kotting, C., Gerwert, K., and Hofmann, E. (2012) Time-resolved Fourier Transform Infrared Spectroscopy of the Nucleotide-binding Domain from the ATP-binding Cassette Transporter MsbA: ATP hydrolysis is the rate-limiting step in the catalytic cycle. *J. Biol. Chem. 287*, 23923−23931.
(33) Janas, E., Hofacker, M., Chen, M., Gompf, S., van der, D. C., and Tampé, R. (2003) The ATP hydrolysis cycle of the nucleotide-binding domain of the mitochondrial ATP-binding cassette transporter Mdl1p. *J. Biol. Chem. 278*, 26862−26869.
(34) Lewis, H. A., Buchanan, S. G., Burley, S. K., Conners, K., Dickey, M., Dorwart, M., Fowler, R., Gao, X., Guggino, W. B., Hendrickson, W. A., Hunt, J. F., Kearins, M. C., Lorimer, D., Maloney, P. C., Post, K. W., Rajashankar, K. R., Rutter, M. E., Sauder, J. M., Shriver, S., Thibodeau, P. H., Thomas, P. J., Zhang, M., Zhao, X., and Emtage, S. (2004) Structure of nucleotide-binding domain 1 of the cystic fibrosis transmembrane conductance regulator. *EMBO J. 23*, 282−293.
(35) Oswald, C., Holland, I. B., and Schmitt, L. (2006) The motor domains of ABC-transporters. What can structures tell us? *Naunyn-Schmiedeberg's Arch. Pharmacol. 372*, 385−399.
(36) Zaitseva, J., Jenewein, S., Jumpertz, T., Holland, I. B., and Schmitt, L. (2005) H662 is the linchpin of ATP hydrolysis in the nucleotide-binding domain of the ABC transporter HlyB. *EMBO J. 24*, 1901−1910.
(37) Smith, P. C., Karpowich, N., Millen, L., Moody, J. E., Rosen, J., Thomas, P. J., and Hunt, J. F. (2002) ATP binding to the motor domain from an ABC transporter drives formation of a nucleotide sandwich dimer. *Mol. Cell 10*, 139−149.
(38) McRee, D. E. (2004) Differential evolution for protein crystallographic optimizations. *Acta Crystallogr., Sect. D: Biol. Crystallogr. 60*, 2276−2279.
(39) Mittal, A., Böhm, S., Grütter, M. G., Bordignon, E., and Seeger, M. A. (2012) Asymmetry in the homodimeric ABC transporter MsbA recognized by a DARPin. *J. Biol. Chem. 287*, 20395−20406.
(40) Zaitseva, J., Oswald, C., Jumpertz, T., Jenewein, S., Wiedenmann, A., Holland, I. B., and Schmitt, L. (2006) A structural

analysis of asymmetry required for catalytic activity of an ABC-ATPase domain dimer. *EMBO J. 25*, 3432−3443.
(41) Tina, K. G., Bhadra, R., and Srinivasan, N. (2007) PIC: Protein Interactions Calculator. *Nucleic Acids Res. 35*, W473−W476.
(42) Wallace, A. C., Laskowski, R. A., and Thornton, J. M. (1995) LIGPLOT: a program to generate schematic diagrams of protein-ligand interactions. *Protein Eng. 8*, 127−134.
(43) Tombline, G., Muharemagić, A., White, L. B., and Senior, A. E. (2005) Involvement of the "occluded nucleotide conformation" of P-glycoproein in the catalytic pathway. *Biochemistry 44*, 12879−12886.
(44) Orelle, C., Gubellini, F., Durand, A., Marco, S., Lévy, D., Gros, P., Di Pietro, A., and Jault, J. M. (2008) Conformational change induced by ATP binding in the multidug ATP-binding cassette transporter BmrA. *Biochemistry 47*, 2404−2412.
(45) Moody, J. E., Millen, L., Binns, D., Hunt, J. F., and Thomas, P. J. (2002) Cooperative, ATP-dependent association of the nucleotide binding cassettes during the catalytic cycle of ATP-binding cassette transporters. *J. Biol. Chem. 277*, 21111−21114.
(46) Verdon, G., Albers, S. V., van, O. N., Dijkstra, B. W., Driessen, A. J., and Thunnissen, A. M. (2003) Formation of the productive ATP-Mg2+-bound dimer of GlcV, an ABC-ATPase from Sulfolobus solfataricus. *J. Mol. Biol. 334*, 255−267.
(47) Ward, A., Reyes, C. L., Yu, J., Roth, C. B., and Chang, G. (2007) Flexibility in the ABC transporter MsbA: Alternating access with a twist. *Proc. Natl. Acad. Sci. U. S. A 104*, 19005−19010.
(48) Aller, S. G., Yu, J., Ward, A., Weng, Y., Chittaboina, S., Zhuo, R., Harrell, P. M., Trinh, Y. T., Zhang, Q., Urbatsch, I. L., and Chang, G. (2009) Structure of P-glycoprotein reveals a molecular basis for poly-specific drug binding. *Science 323*, 1718−1722.
(49) Hohl, M., Briand, C., Grütter, M. G., and Seeger, M. A. (2012) Crystal structure of a heterodimeric ABC transporter in its inward-facing conformation. *Nat. Struct. Mol. Biol. 19*, 395−402.